Expansion, functional diversification and gene fusion events in the Ato protein family

Faezeh Ghasemi [1,2], Cláudia Barata-Antunes [1,2], Yiannis Pyrris[3,4], Patrícia Ataíde[1,2], João Alves[1,2], Vitor Fernandes[1,2], Rosana Alves[1,2], Alexandra Gomes-Gonçalves[1,2], Margarida Casal [1,2], Wouter Van Genechten[5], Jana Nysten[5], Alistair J. P. Brown[6], Patrick Van Dijck[5], George Diallinas[3,4], Alexandros A Pittis[3], Isabel Soares-Silva[1,2], Sandra Paiva[1,2*]

[1] Centre of Molecular and Environmental Biology, Department of Biology, University of Minho, Braga, Portugal.
[2] Institute of Science and Innovation for Bio-Sustainability (IB-S), University of Minho, Braga, Portugal.
[3]Institute of Molecular Biology and Biotechnology of the Foundation for Research and Technology, 70013, Heraklion, Greece.
[4]Department of Biology, National and Kapodistrian University of Athens, Panepistimiopolis 15784, Athens, Greece.
[5] Laboratory of Molecular Cell Biology, Institute of Botany and Microbiology, K.U. Leuven, Leuven, Belgium.
[6] MRC Centre for Medical Mycology, University of Exeter, Exeter, England, UK

* Corresponding author
Email: spaiva@bio.uminho.pt

Author Contributions:

FG performed the lab experiments and was responsible for the *in-silico* analysis, curation, analysis and visualisation of the data. **CBA** was actively involved in this work, and made important contributions to the experiments, particularly in Western blot, analysis and visualisation of data. **YP** performed Bioinformatics and phylogenetic analysis. **PA** was actively involved in the lab work and made important contributions to the experiments, particularly in Western blot and DNA cloning. **JA, VF** and **MC** contributed to the Bioinformatics analysis. **RA** assisted in the mutant's constructions. **AG, WVG, JN** and **PVD** contributed to construction of **GFP** fusions. **ISS**, **AAP**, **GD** and **AJPB** contributed to conceptualization, validation, and supervision. **SP** and **PVD** contributed to funding acquisition, conceptualization, validation and supervision. **FG** drafted the original manuscript with additional input from all authors.

Competing Interest Statement: The authors declare no competing interests or financial conflicts related to the content of this article.
Classification: Original Research Article
Keywords: *Candida albicans,* plasma membrane proteins, carboxylic acids.

Abstract

Candida albicans, a commensal opportunistic pathogen, exhibits remarkable metabolic flexibility and adaptability to environmental changes. In glucose-limited niches, it utilizes alternative carbon sources such as carboxylic acids, which may influence its pathogenicity. In *Saccharomyces cerevisiae*, the uptake of monocarboxylates occurs through regulated plasma membrane (PM) transport proteins, such as Ato1 (Ady2), which belongs to the Acetate Uptake Transporter (AceTr) family. In *C. albicans*, these proteins are notably expanded, consisting of ten Ato-like proteins (ATO1-ATO10), whose functions remain unknown.

Here, we investigated the role of Ato proteins in carboxylic acid utilization by *C. albicans* using *in-silico* and functional analysis. Our data revealed that several *C. albicans* Atos retain conserved AceTr motifs but possess distinct structural features, including differences in pore radius and binding sites for acetate and lactate. Expression analysis revealed that Ato1, Ato2, Ato3, and Ato6 exhibit distinct cellular localization and expression levels on the plasma membrane, depending on the presence or absence of monocarboxylates. Remarkably, deletion of *ATO1* impaired *ATO2* and *ATO3* expression and caused ER retention of a distinct form of Ato2, suggesting a central regulatory role for Ato1 in the Ato transport system. Finally, we identified a novel Ato-related protein family in vertebrates. This family has three consecutive 6-helix transport domains and a unique C-terminal fusion with Sua5/YciO/YrdC, an enzyme involved in tRNA modification.

Overall, our data suggests that the Ato protein family might play a critical role in the utilization of acetic or lactic acids in *C. albicans*. It also proposes potential functional redundancy among its members, which may contribute to rapid environmental adaptation and pathogenicity.

52 **1. Introduction**

53 Opportunistic fungal pathogens of humans include several *Candida* species that have become serious
54 threats to global public health (1–4). These fungi can cause a broad spectrum of diseases, ranging from
55 superficial infections of the vaginal and oral mucosa to life-threatening systemic infections (5,6). The
56 genus *Candida* comprises 200 species, with approximately 10% identified as human pathogens (7). The
57 most clinically significant species include *C. albicans*, *C. glabrata*, C. *auris*, *C. tropicalis*, *C. parapsilosis* and
58 *C. krusei* (8–12). *C. albicans,* a commensal microorganism, exhibits the capacity to colonize various niches
59 of the host, such as skin, oral cavity, gastrointestinal tract, and urogenital tract (13–15). Considerable
60 metabolic flexibility underlies this adaptability (16,17).

61 Although sugars are preferred carbon sources for *C. albicans* (18)*,* this pathogen can rapidly adapt to
62 glucose-limited environments, such as the vaginal and gastrointestinal tracts (19,20). In these niches, *C.*
63 *albicans* cells can utilize alternative carbon sources such as carboxylic acids (lactate, acetate, succinate,
64 butyrate or propionate), amino acids and N-acetylglucosamine, which are produced by host cells or the
65 resident microbiota (16,20–23). Carboxylic acids exist in two forms depending on their pKa and the
66 ambient pH. When the environmental pH is lower than the pKa, the protonated (undissociated) form of
67 acid can cross the plasma membrane by passive diffusion. Conversely, when the pH exceeds the acid's
68 pKa, the acid is predominantly in its anionic (dissociated) form, requiring protein mediated systems to
69 cross the plasma membrane (24,25).

70 The Acetate Uptake Transporter (AceTr) family (TCDB 2.A.96, Pfam: PF01184) is evolutionarily conserved
71 across bacteria, archaea and fungi (26). A majority of fungal genomes (97 %) include members of this
72 family, suggesting crucial roles in fungal growth and development (27,28). Key transporters of the AceTr
73 family include Gpr1 in *Yarrowia lipolytica* (29), Ady2/Ato1 in *Saccharomyces cerevisiae*, AcpA in *Aspergillus*
74 *nidulans* (30) and Satp in bacteria (31). Members of the AceTr family carry six transmembrane segments
75 (TMS). The conserved signature motif NPAPLGL(M/F) at the beginning of the first transmembrane
76 segment (TMS) plays a critical role in substrate uptake (26,32). The only elucidated crystal structures
77 among AceTr family members are those of SatP from *Escherichia coli* (EcSatP) and *Citrobacter koseri*
78 (SkSatP) (33,34). Structural analysis of SatP has confirmed six transmembrane helices, four substrate-
79 binding sites, and a constriction site located in the center of the protein pore. This constriction site is
80 formed by three hydrophobic residues, phenylalanine (F), tyrosine (Y), and leucine (L), known as the FLY
81 motif (structural element) which is essential in substrate selectivity and specificity (32,33).

82 In *Esherichia coli*, EcSatp facilitates the transport of monocarboxylates (acetate and lactate) and
83 dicarboxylate (succinate) (31–33). In *S. cerevisiae*, Ato1, is identified as an acetate permease with

84 additional capability of transporting monocarboxylates, including propionate, formate and lactate (26,30).
85 and has two paralogs: Ato2 (or Fun34) and Ato3. The expression of these three transporters is induced
86 significantly under carbon-limiting conditions and following entry to stationary phase after growth on
87 glucose (35,36). Palková et al., 2002 reported that the ScAto transporters (Ato1, Ato2, and Ato3) drive
88 increases in the external pH by expelling ammonium and importing protons. The *ScATO1* gene is also
89 required for protein-mediated acetate import, when *S. cerevisiae* cells are grown in acetate at pH 6.0 (30).
90 Homologs of *ScATO1* have been found in *Candida* species. Indeed, twelve of the most medically relevant
91 Candida spp. contain at least two homologous genes, and the majority have five or more. The expanded
92 *ATO* gene families in *Candida* pathogens reinforces the idea that they play important roles in fungal
93 adaptation and probably contribute to virulence (8,26). *C. albicans*, has a large AceTr family that includes
94 ten *ATO* (Acetate Transporter Ortholog) genes (ATO1, ATO2, ATO3, ATO4, ATO5, ATO6, ATO7, ATO8,
95 ATO9, and ATO10)(8). The functions of the respective proteins remain largely unknown (37). *CaATO9* and
96 *CaATO10* are probably pseudogenes, originated from a single gene that was disrupted by insertion of
97 transposable element (8). Previous studies have shown that the neutralization of the acidic
98 phagolysosome induces the differentiation of *C. albicans* yeast cells to form filamentous hyphae, thereby
99 facilitating their escape from macrophages via immune cell rupture (38). Notably, mutations in certain *C.*
100 *albicans ATO* genes disrupt this process, impairing phagolysosomal neutralization, hyphal differentiation,
101 and macrophage killing (37). In a murine model of gut colonization, deletion of the entire *ATO* gene family
102 significantly reduces *C. albicans* colonization, particularly after antibiotic elicited bacterial disruption,
103 indicating that *ATOs* are important for long-term persistence in the gut (Alves et al., 2025, unpublished
104 data, manuscript under review).
105 In this study, we focused on the phylogenetic analysis of AceTr family members, the *in silico* structural
106 characterization of Ato proteins divergent *Candida* species (*C. albicans, C. glabrata*, and *C. auris*), and the
107 cellular expression of CaAto proteins. Our analysis reveals the conservation of significant AceTr specific
108 motifs across the mentioned species alongside the presence of distinct pore radius in the respective Ato
109 proteins, suggestive of distinct transport activities and specificities. Additionally, we show that *ATO1,*
110 *ATO2*, *ATO3* and *ATO6* are differentially expressed in *C. albicans*, with *ATO1* playing a key role in regulating
111 the expression of other Ato family members for the assimilation of short-chain carboxylic acids like acetic
112 and lactic acids. Finally, we describe a previously unknown ATO-related family in vertebrates that exhibits
113 ATO-like transport domains unexpectedly fused to the Sua5/YciO/YrdC domain involved in the formation
114 of threonyl-carbamoyl-adenosine in tRNA modification.

115 ## 2. Methods

116 ### 2.1 *In silico* analysis

117 #### 2.1.1 Protein sequence alignments and phylogenetic construction

118 Entries containing the PFAM annotation Gpr1_Fun34_YaaH (PF01184) were collected from UniprotKB
119 using the Uniprot API. The sequences were aligned using MAFFT-LINSI (39) and positions with >90% gaps
120 were removed from the alignment with TrimAl (40). Trees were constructed using IQtree v2.0 (41) with
121 model selection on auto (selected model: Q.pfam+G4) and 1000 iterations of ultrafast bootstrap. Manual
122 inspection was performed for the fungal trees and almost identical branches (representing the same
123 sequence from different strains of the same species or different proteins isoforms) were removed. Trees
124 were visualized using ETE4 (https://github.com/etetoolkit/ete4) (42) and Adobe Photoshop.
125 The identification of the entire conserved amino acid residues of the AceTr family was performed with
126 the Clustal Omega software (43) (www.clustal.org). The protein sequences of the following AceTr
127 members were included in the multiple sequence alignment: *S. cerevisiae* Ato1, Ato2, Ato3; *C. albicans*
128 Ato1, Ato2, Ato3, Ato4, Ato5, Ato6, Ato7, Ato8; *C. glabrata*: Ato1, Ato2, Ato3 and *C. auris*: Ato1, Ato2,
129 Ato3 (Table 1).

130 #### 2.1.2 Three-dimensional structure and pore radius predictions

131 The 3D structures of Ato proteins from *S. cerevisiae*, *C. albicans*, *C. glabrata* and *C. auris* were obtained
132 from the AlphaFold Protein Structure Database (Table 1)(44,45). These structures were used to predict
133 the radius along the pore using the HOLE program (2.2.005 Linux) (46). The HOLE program provided the
134 Van der Waals *file simple radii*, which was used to predict the pore of each Ato protein. These predictions
135 were visualized along with 3D protein structures by the Visual Molecular Dynamics program (VMD,
136 1.9.3)(47). The pore radius of the Ato proteins was presented on a graphic with the X coordinates
137 representing the length of the Ato proteins (48).

138 #### 2.1.3 Molecular docking

139 Molecular docking simulations with acetate and lactate substrates were performed using Auto Dock Vina
140 from PyRx virtual screening tool (49), as previously described (50). The ligand structure of acetate and
141 lactate were obtained from PubChem (https://pubchem.ncbi.nlm.nih.gov/). The simulated interactions of
142 ligands and proteins were visualized and analyzed by Maestro v11.2 and Chimera, a graphical user

interface for AutoDock Vina (50). The dissociated forms of each carboxylic acid were used in the docking studies.

Table 1. Accession number of Ato proteins of *C. albicans*, *C. glabrata*, *C. auris* and *S. cerevisiae* in NCBI and AlphaFold Databases. The "Database nomenclature" refers to the nomenclature used in NCBI. The "Alias" denotes the nomenclature recently proposed by our group (8). The Alias was used for the analysis performed in this study.

Species	Database nomenclature	Alias (8)	Accession no. in NCBI	Accession no. in AlphaFold Database
C. albicans	*FRP3*	*ATO1*	XP_710295.1	AF-A0A1D8PHP8-F1
	ATO1	*ATO2*	XP_710650.1	AF-A0A1D8PJ22-F1
	ATO2	*ATO3*	XP_718515.2	AF-A0A1D8PJ42-F1
	ATO6	*ATO4*	XP_714701.1	AF-A0A1D8PKA0-F1
	ATO5	*ATO5*	XP_714703.1	AF-A0A1D8PKD7-F1
	FRP6	*ATO6*	XP_716748.1	AF-Q5A4K0-F1
	FRP5	*ATO7*	XP_716747.2	AF-A0A1D8PPM3-F1
	ATO7	*ATO8*	XP_019330752.1	AF-A0A1D8PGM7-F1
	ATO9	*ATO10*	XP_717951.1	AF-Q5A867-F1-v4
	ATO10	*ATO9*	XP_717953.1	AF-Q5A865-F1-v4
C. glabrata	*ATO1*	-	XP_449497.1	AF-Q6FJU7-F1
	ATO2	-	XP_449115.1	AF-Q6FKX9-F1
	ATO3	-	XP_444907.1	AF-Q6FYA8-F1
C. auris	*ATO1*	-	XP_028889701.1	AF-A0A2H0ZYE7-F1
	ATO2	-	XP_028890140.1	AF-A0A2H0ZRA6-F1
	ATO3	-	XP_028890274.1	AF-A0A2H0ZM18-F1
S. cerevisiae	*ATO1*	-	NP_009936.1	AF-A0A815X247-F1
	ATO2	-	NP_014399.3	AF-C7GLQ2-F1
	ATO3	-	NP_010672.1	AF-A0A815XMT5-F1

2.1.4 Domain annotation

Domains were predicted using Hmmscan (HMMER 3.4, Aug 2023; http://hmmer.org/) for the HMM-profiles of interest (PF01184: Gpr1_Fun34_YaaH and PF01300: Sua5_yciO_yrdC). Hits with a bit-score > 25 for PF01300 and > 0 for PF01184 (increasing sensitivity to predict some of the more divergent metazoan domains) were considered. Domains were visualized next to the trees using ETE4.

155 **2.1.5 Structural superimposition and visualization**

156 The crystal structure for SatP (33) (5ZUG) and an Alphafold 2.0 predicted structure for A0A3B3D9A3 (44)
157 were used. Structures were superimposed using the TM-align webserver (https://zhanggroup.org/TM-
158 align/) for TM-score and RMSD inference. For visualization PyMOL (Version 3.0 Schrödinger, LLC) was used.
159 Structures were superimposed using the PyMOL super command and figures were finalized using Adobe
160 Photoshop.

161 **2.1.6. Phosphorylation sites prediction**

162 Phosphorylation site prediction was performed using Netphos-3.1b
163 (https://services.healthtech.dtu.dk/services/NetPhos-3.1/) (51,52). This tool uses multiple neural
164 networks to make predictions.

165 **2.2 Strains and growth conditions**

166 All *C. albicans* strains generated in this study, listed in Table 2, were derived from the wild-type (WT)
167 clinical isolate *C. albicans* SC5314. Strains generated using the CRISPR-Cas9 system were selected on YPD
168 medium supplemented with 200 µg/mL nourseothricin. Following the removal of the CRISPR-Cas9
169 cassette, the strains were cultured on yeast extract-peptone-dextrose (YPD) medium, comprising yeast
170 extract (1% w/v), peptone (1% w/v), glucose (2% w/v), and agar (2% w/v). For microscopy analysis, cells
171 were grown in synthetic minimal medium (SM: 0.67% w/v YNB with ammonium sulphate) containing 0.2%
172 glucose and then transferred to synthetic minimal medium supplemented with specific carboxylic acids:
173 acetate (0.1% v/v, pH 6.0) or lactate (0.1% v/v, pH 5.0) at 30 °C. The pH of the media containing carboxylic
174 acids was adjusted with a 5 M NaOH solution.

175 **2.3 Genetic manipulation of *C. albicans* using the CRISPR-Cas9 system for generation of GFP**
176 **fusions and gene deletions**

177 GFP fusions at the 3' terminal of *ATO* genes were performed using the CRISPR-Cas9 system following an
178 adapted version of the protocol from Hernday lab (53). In summary, each gene's customized gRNA
179 expression cassette (Fragment C) was generated by assembling fragments A and B using cloning-free
180 stitching PCR (with primers AH01237 and AH01236). Fragment A was amplified from pADH110 (with
181 AHO1096 and AH1098 primers), while fragment B was amplified from pADH147 (with AHO1097 and
182 Hernday-GOI primers). The Cas9 cassette was obtained by digestion of the pADH99 plasmid with the *MssI*
183 restriction enzyme. In a single transformation, the Cas9 and gRNA cassettes were co-transformed along

184 with a specific donor's DNA-GFP (linear DNA fragment), which was amplified from the template CIp10 -
185 γmGFP (with primers dDNA-GOI-GFP-FW and dDNA-GOI-GFP-RV) (54). *C. albicans* positive transformants
186 were selected on YPD medium supplemented with nourseothricin and verified by colony PCR (with desired
187 gene-FW-check and desired gene-RV-check or Inside-GFP-Check-RV primers). After confirming GFP
188 integration, the NAT marker, Cas9, and gRNA expression cassettes were removed by inducing the maltose-
189 inducible FLP recombinase system in YP medium with 3% maltose, followed by overnight incubation at 30
190 °C. To verify the effective removal of CRISPR components, cells were streaked onto YPD agar to isolate
191 single colonies. They were then tested on both YPD and YPD supplemented with nourseothricin. Next, all
192 generated strains were further tested by colony PCR and confirmed through sequencing. *C. albicans ATO-*
193 *GFP* strains, carrying a single *ato* knockout, were generated using a modified transient CRISPR-Cas9
194 approach (55). All sgRNA expression cassettes were constructed through a three-step PCR process using
195 the pV1093 plasmid as a template. The steps included (i) synthesizing the SNR52 promoter (with
196 oligonucleotides: SNR52/F and SNR52/R-desired gene), (ii) generating the gRNA scaffold (with primers:
197 sgRNA/F-desired gene, and sgRNA/R) and (iii) fusing the SNR52 promoter with gRNA scaffold cassettes
198 (with oligonucleotides: SNR52/N and sgRNA/N). The Cas9 expression cassette was amplified from the
199 pV1093 plasmid via PCR using the CaCas9/F and CaCas9/R primers. Similarly, repair templates specific to
200 the desired gene were generated through PCR using the primers NAT-desired gene-repair/F and NAT-
201 desired gene-repair/R. *C. albicans* cells were simultaneously transformed with the three constructed
202 cassettes using the classical lithium acetate method (56). Positive *C. albicans* transformants were selected
203 in YPD supplemented with nourseothricin and, subsequently, validated through colony PCR (using the
204 specific oligonucleotides gene-FW-check and desired gene-RV-check). All primers used in this study are
205 listed in Table S1**.**

206 **Table 2. List of strains used in this study**

Strain	Genotype	Source
WT	SC5314	-
ATO1-GFP (FG16-19)	*ATO1*-GFP/*ATO1*-GFP	This study
ATO2-GFP (FG08-11)	*ATO2*-GFP/*ATO2*-GFP	This study
ATO3-GFP (FG12-15)	*ATO3*-GFP/*ATO3*-GFP	This study
ATO4-GFP (FG52-54)	*ATO4*-GFP/*ATO4*-GFP	This study
ATO5-GFP-Herto (FG65-67)	*ATO5*-GFP/*ATO5*	This study
ATO6-GFP (FG55-56)	*ATO6*-GFP/*ATO6*-GFP	This study
ATO7-GFP (FG25-32)	*ATO7*-GFP/*ATO7*-GFP	This study
ATO8-GFP (FG59-64)	*ATO8*-GFP/*ATO8*-GFP	This study
ATO9-GFP (FG71-73)	*ATO9*-GFP/*ATO9*-GFP	This study
ATO10-GFP (FG74-76)	*ATO10*-GFP/*ATO10*-GFP	This study
ATO1-GFP/*ato2Δ* (RA42-44)	*ATO1*-GFP//*ato2*::NAT//*ato2*::NAT	This study
ATO3-GFP/*ato1Δ* (RA45-47)	*ATO3*-GFP//*ato1*::NAT//*ato1*::NAT	This study
ATO3-GFP/*ato2Δ* (RA48-50)	*ATO3*-GFP//*ato2*::NAT//*ato2*::NAT	This study
ATO2-GFP/*ato1Δ* (RA52-54)	*ATO2*-GFP//*ato1*::NAT//*ato1*::NAT	This study

ATO1-GFP/*ato3Δ* (PA19-23)	*ATO1*-GFP//*ato3*::NAT//*ato3*::NAT	This study
ATO2-GFP/*ato3Δ* (PA24-26)	*ATO2*-GFP//*ato3*::NAT//*ato3*::NAT	This study

2.4 Epifluorescence microscopy

C. albicans cells expressing Atos-GFP were grown in a synthetic minimal medium supplemented with 0.2% glucose until the exponential phase at 30 °C, 200 rpm. Cells were then washed and transferred to synthetic minimal media containing acetate (0.1% v/v, pH 6.0), lactate (0.1% v/v, pH 5.0), or without carbon source at 30 °C, 200 rpm. Samples were collected at 0 hours, 5 hours, and 24 hours after derepression for analysis by epifluorescence microscopy and for further protein extraction (see section 2.5). For microscopy analysis, 1 mL of each culture was harvested, cells were concentrated by centrifugation and manually immobilized on slides. Cells were visualized using a Leica DM5000B microscope with appropriate filters. Images were captured with a Leica DFC 350FX R2 digital camera using LAS AF V1.4.1 software (Leica). The images presented are representative of three independent experiments.

2.5 Western Blot and quantification analysis

Yeast cells were grown as explained above in section 2.4. At the time-point 5 hours, cells were harvested at a final OD_{640} of 1.5 per mL, and total protein extracts were prepared using the NaOH/TCA method (57). Briefly, cells were harvested by centrifugation (max. rpm, 1 min, 4 °C) and the pellet was resuspended in 500 µL of cold water. Cell lysates were prepared by adding 50 µL of NaOH (1.85 M) following 10 min of incubation on ice. Then, 50 µL of trichloroacetic acid (TCA, 50%) was added and the samples were incubated for an additional 10 min on ice. Protein precipitates were collected by centrifugation (max. rpm, 15 min, 4 °C). The pellets were dissolved in 50 µL of loading buffer (33.3 mM Tris-hydrochloride pH 6.8; 1.33 mM EDTA; 1.33% sodium dodecyl sulphate (SDS); 6.66% glycerol; 0.02% bromophenol blue and 2% Beta-mercaptoethanol) and heated at 37 °C for 10 min. Each sample (10 µL) was loaded onto a 10% acrylamide gel. Following electrophoresis, the separated proteins were transferred onto nitrocellulose membranes (GE Healthcare Life Sciences. For transference and loading controls, the membranes were stained with a Ponceau S solution (0.1% Ponceau (w/v); 0.5% glacial acetic acid (v/v)). Following washing and blocking steps, the membranes were probed with the primary antibody anti-GFP (monoclonal, mouse IgG1κ, clones 7.1 and 13.1, Roche, 11814460001) used at 1:3000 dilution. The antimouse-IgG (whole molecule)-peroxidase produced in rabbit (A9044, Sigma) was used as a secondary antibody at 1:100000 dilution. The signal was detected by enhanced chemiluminescence using the WesternBright ECL HRP substrate (advansta). All images were captured using a Syngene G:Box Chemi XX9 image documentation system and GeneSys software. The quantification levels of the GFP signal were performed using the ImageJ

237 software (version 1.53k). The data is represented in arbitrary units (A.U.) as the mean of at least three
238 independent experiments (n≥3) (Figure S8). The error bars represent the standard error of the mean (SEM)
239 (Prism 8.0; GraphPad software, version 8.0.1).

240 **3. Results and Discussion**

241 **3.1 *C. albicans* Ato Members possess conserved NPAPLGL, FLY and SY[F]GFW motifs**

242 Multiple sequence alignment of AceTr members from *S. cerevisiae*, *C. albicans*, *C. glabrata* and *C. auris*
243 showed that CaAto1-8, CgAto1-3, CauAto1-3 and ScAto1-3 contain common conserved regions (Figure 1).
244 *C. albicans* Ato9 and Ato10 were excluded from this analysis as they are likely functionally inactive (8).
245 However, manually fusing CaAto9 (2 TMS near the N-terminus) and CaAto10 (4 TMS near the C-terminus)
246 sequences does yield a structure similar to other *C. albicans* Atos (Figure S1) which may suggest that they
247 represent fragments of one single gene. Notably, the putative functional $N^{88}PAPLGL^{94}$ signature motif
248 (numbering refers to CaAto-1), which is localized at the beginning of the first TMS (Figure S2), is fully
249 conserved in CaAto1-3, CgAto1-2, CauAto2, and ScAto1-2 (Figure 1). In CaAto6-8 and CauAto3, the first
250 Pro residue in this motif (Pro89) is substituted by Ala or Ser. In addition, in CaAto4-7 and CauAto3, the
251 second Pro residue (Pro91) is substituted by Ala. The highly conserved residue Leu92 is substituted by
252 isoleucine in CaAto4 and CaAto5 and valine in CaAto7. Therefore, CaAto7 and CaAto8 exhibit the highest
253 divergence in the NPAPLGL motif of these ATO families, differing in four and three of the sixteen residues
254 in this motif, respectively. These differences are likely to change the substrate affinities, specificities
255 and/or activities of these transporters. This prediction is based on previous mutational analyses of ScAto1,
256 which established that amino acid substitutions in this motif impaired protein function *per se*, without
257 affecting its proper localization to the plasma membrane (50).
258 In ScAto1, the narrowest constriction site is formed by the FLY structural element. Previous studies have
259 demonstrated that mutations of FLY residues of ScAto1 lead to altered protein activity and specificity,
260 highlighted by the observation that Leu219Ala allows cells to grow on succinic acid (32). All analyzed
261 *Candida* homologs possess a well-conserved phenylalanine in this FLY motif (Phe98, Figure 1), with the
262 exception of CaAto4 and CaAto5, where it has been substituted by threonine. The substitution of a bulky
263 hydrophobic residue by a polar amino acid might influence substrate transport through the inner pore of
264 the transporter, as previously described for ScAto1 (32). The Tyr residue of the FLY motif is also highly
265 conserved, being replaced by phenylalanine, a residue with similar biochemical character, in ScAto2,
266 ScAto3, CgAto2, CgAto3, and CauAto3 (Figure 1). Finally, the Leu residue of the FLY motif is nearly

absolutely conserved with the only exception of CaAto4, where it is a Tyr. Also, the Tyr residue of the FLY structural motif is also part of the SY[F]GFW linear signature motif of the AceTr family, located in TMS3 (Figure S2). This motif is also highly conserved among the Ato proteins examined. Overall, our *analysis* suggests that conserved evolutionary substitutions in the NPAPLGL, FLY and SY[F]GFW motifs might have resulted in modulations of transport activity and/or substrate specificity of Ato proteins in these *Candida* pathogens.

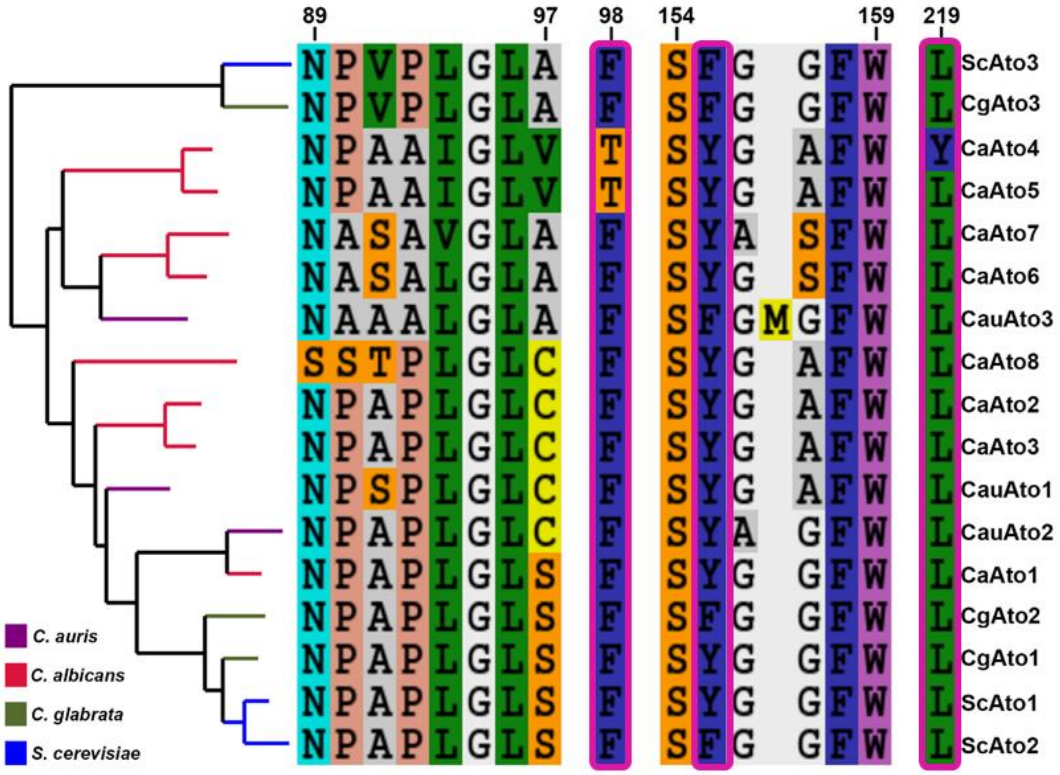

Figure 1. Phylogeny and important positions of Ato homologous sequences from *C. albicans* (Ato1-8), *C. glabrata* (Ato1-3), C. auris (Ato1-3) and *S. cerevisiae* (Ato1-3). The signature motif, N-P-A-P-L-G-L of the AceTr family (58), the narrowest hydrophobic constriction region (FLY) (pink rectangles) (33) and the signature motif S-Y[F]-G-F-W are aligned next to the tree. Full alignment is available in the supplementary data (Figure. S2).

3.2 *C. albicans* Atos have distinct pore radius

The pore radii of Ato proteins in *C. albicans*, *C. glabrata* and *C. auris* were predicted to determine the putative translocation paths for their substrates (e.g. acetate or lactate) (Figure 2). The narrowest constriction in each path is located around the FLY region (Figure 2A). In CaAto4 the pore seems to be blocked in this region, due to the existing substitutions in the FLY motif. Additionally, CaAto4 includes an additional restriction site located in the upper region of the protein, that faces the extracellular medium, specifically near the residues Phe94, Phe150, and Phe218. Also, the central pore of CaAto7 appears blocked despite the conservation of FLY motif. This blockage may be caused by variations in the amino

286 acid residues that interact with the closet transmembrane segment (TMS). On the other hand, there is a
287 widening of the pore around the FLY motif of CaAto5 due to a substitution to TLY in this protein. In fact,
288 the narrowest constriction site of CaAto5 is found in the upper section of the protein facing the
289 extracellular space (Phe93, Phe149, and Phe217), similar to the second constriction site of CaAto4. An
290 additional constriction to the FLY region has been predicted for CgAto2 and CauAto1, closer to the
291 extracellular region (Figure S3, A, B).
292 The variations in pore radius between CaAto4, CaAto5, CaAto7 and CaAto8 compared to ScAto1 and
293 CaAto1(Figure 2B) suggest that these proteins might possess altered transport activity or specificity
294 compared to ScAto1 or CaAto1. The reduction of the pore radius in CaAto4 and CaAto7 might result in the
295 uptake of only small carboxylic acids such as formate or , or is suggestive of a signaling rather than
296 transport role. Indeed, Rendulic and colleagues (2021) found that the substitution of Leu219 with
297 tryptophan (L219W) in the Ato1 mutant *S. cerevisiae* strain led to a reduction of the pore radius at the
298 construction site thereby blocking transport of carboxylic substrates. Therefore, a larger side-chain at this
299 position can arrest transport. Furthermore, the pore radius of CaAto5 in the FLY motif region is wider
300 compared to ScAto1 and CaAto1, suggesting that CaAto5 may be capable of transporting larger molecules,
301 such as succinate and citrate. Indeed, Phe98Ala and Leu219Ala mutations in ScAto1 reduce the
302 constriction at the central FLY region and enable the transport of larger molecules, such as succinate (32).
303 In addition, Tyr155Phe and Leu219Val substitutions in the FLY motif of *Candida jadinii* Ato5, a broad range
304 carboxylate transporter that transports mono- di and tricarboxylates, including citrate (58). These findings
305 indicate that constrictive FLY amino acids play a crucial role in the substrate selectivity and transport
306 activity of Ato transporters.
307 We also identified significant variations between CaAto5, CaAto4 and CaAto7 in their pore radii around
308 the NPAPLGL(M/F) and SYG(X)FW motifs (Figure 1, 2). Also, the pore size prediction displays distinct
309 dissimilarities in the pore radius of CaAto8, not only in the constriction site, but also in the conservation
310 motif region (Figure 2B), which is less well conserved in CaAto8 (Figure 1). On the other hand, given the
311 similarities in structure, pore size and conserved motifs, CaAto1, 2, 3, 6 may transport similar substrates
312 to ScAto1.
313 The pore size analysis of the *C. glabrata* Atos shows that CgAto2 contains two distinct constriction sites
314 (Figure S3, A, C). No significant variation in pore radius was observed between the Atos of *C. glabrata*.
315 However, significant differences in pore radius were identified between *C. auris* CauAto1-2 and CauAto3
316 (Figure S3, D). The extracellular loop regions that link transmembrane segments in CauAto3 are

317 significantly shorter than those in CauAto1-2, leading to dissimilarity in their 3D structures and pore sizes.
318 In addition, the pore radius analysis shows two constriction sites for CauAto1 (Figure S3, B).
319 *S. cerevisiae* strains harbouring wild-type *ATO3* and *ATO2* genes are unable to grow on lactic acid, whereas
320 *ATO2*^{T653C} and *ATO3*^{T284C} mutants can grow on this carboxylic acid (59). Therefore, enlarging the
321 hydrophobic constrictions in these Ato transporters appears to have empowered lactate assimilation by
322 *S. cerevisiae*. Increased binding affinity may also have contributed to an enhanced transport capacity by
323 facilitating ligand passage through the structure. Amino acid residues outside the constriction pore may
324 also have increased transport capacity, for example by stabilising the transporter in the plasma membrane
325 or enhancing transitions between its closed and open states.
326

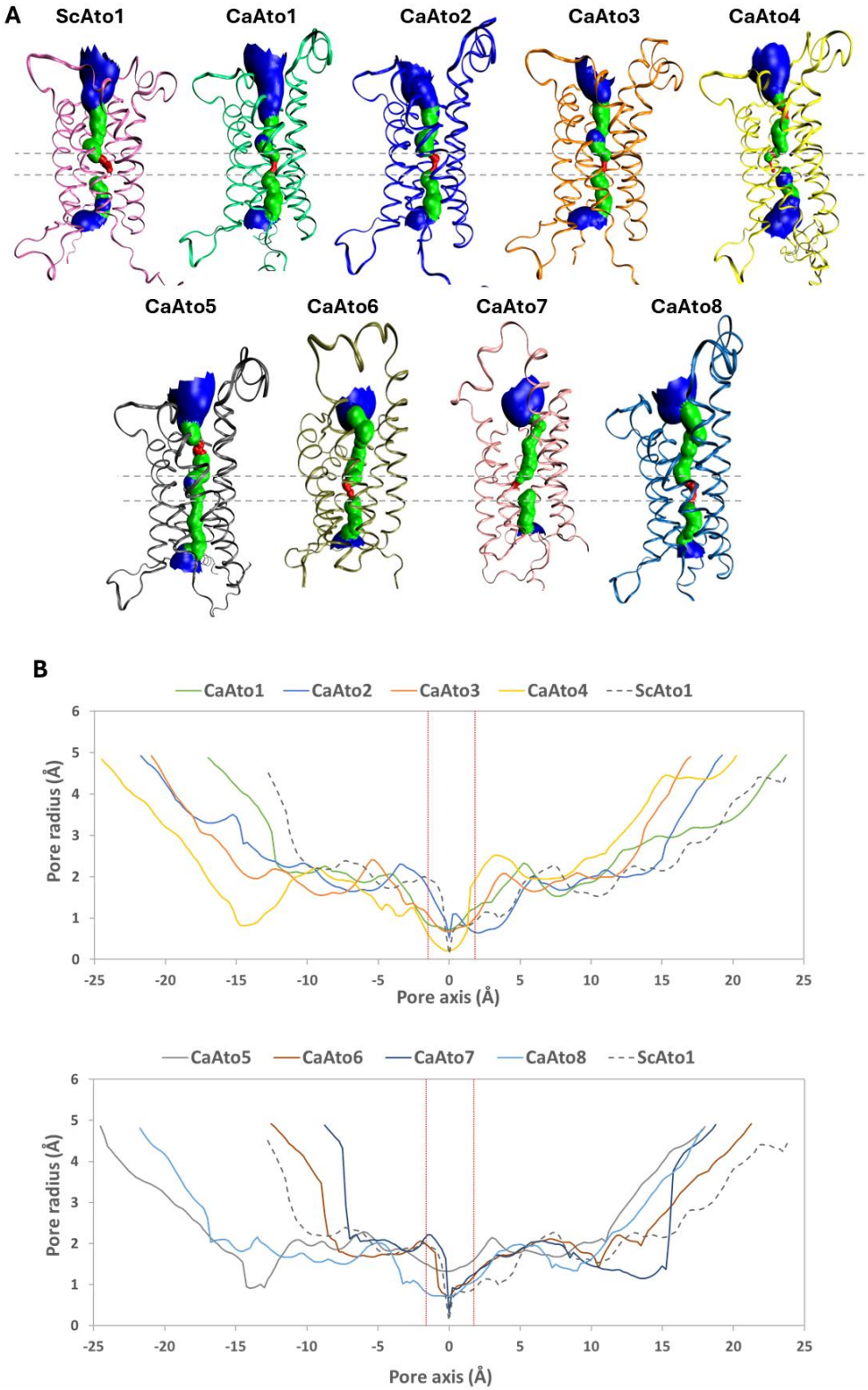

Figure 2. Pore 3D structure predictions and radius profiles simulations along the channel axis in the Atos of *S. cerevisiae* and *C. albicans*. A. Pore 3D structure prediction of ScAto1 and CaAto1-8. The 3D structures of proteins are represented in New Ribbons, with the color scheme consists of blue (representing a bigger pore size), green (representing an intermediate pore size),

and red (representing a more constricted pore size) in pore prediction. The horizontal dashed grey lines correspond to the constricted site where the pore radius is tight. **B.** Simulations for the pore radius profiles along the channel axis in the ScAto1 and CaAto1-8. The region in the middle of proteins that contains the construction site is marked by vertical red dashed lines.

3.3 Acetate and lactate are potential substrates for *C. albicans* Ato1, Ato2, Ato3 and Ato6

The crystal structures of EcSatP and CkSatP indicate a hexameric anion channel (33,34). Each monomer comprises six transmembrane helices and four acetate binding sites aligned along the pore. Acetate binding site S1 faces the cytoplasm, sites S2 and S3 are located inside the main pore surrounding the FLY motif, and site S4 faces the periplasm (34). The FLY motif is located centrally in the pore of the EcSatP monomer, between S2 and S3 sites, leading to the formation of an hourglass-shaped structure.

We performed substrate docking with acetate and lactate for Ato proteins of *S. cerevisiae*, *C. albicans*, *C. glabrata* and *C. auris* Atos using Dock Vina from PyRx virtual screening tool. This revealed at least four predicted binding sites along the channel axis of all proteins we tested (Figure 3 and Figure S4). This was consistent with the crystal structures of the bacterial homologs EcSatP (33) and SkSatP (34). The number and positions of predicted substrate binding sites were similar for all proteins, except for CaAto4, 5, 7, 8 which contained fewer binding sites and theoretically altered binding affinities for acetate and lactate. No acetate and lactate binding sites were identified in the upper region of the CaAto5, suggesting that CaAto5 might not transport acetate or lactate. The molecular docking results for CauAto1 and CauAto3 indicate fewer and distinct binding sites for acetate and lactate, whereas CauAto2 exhibits binding sites nearly identical to other Atos (Figure S4, B).

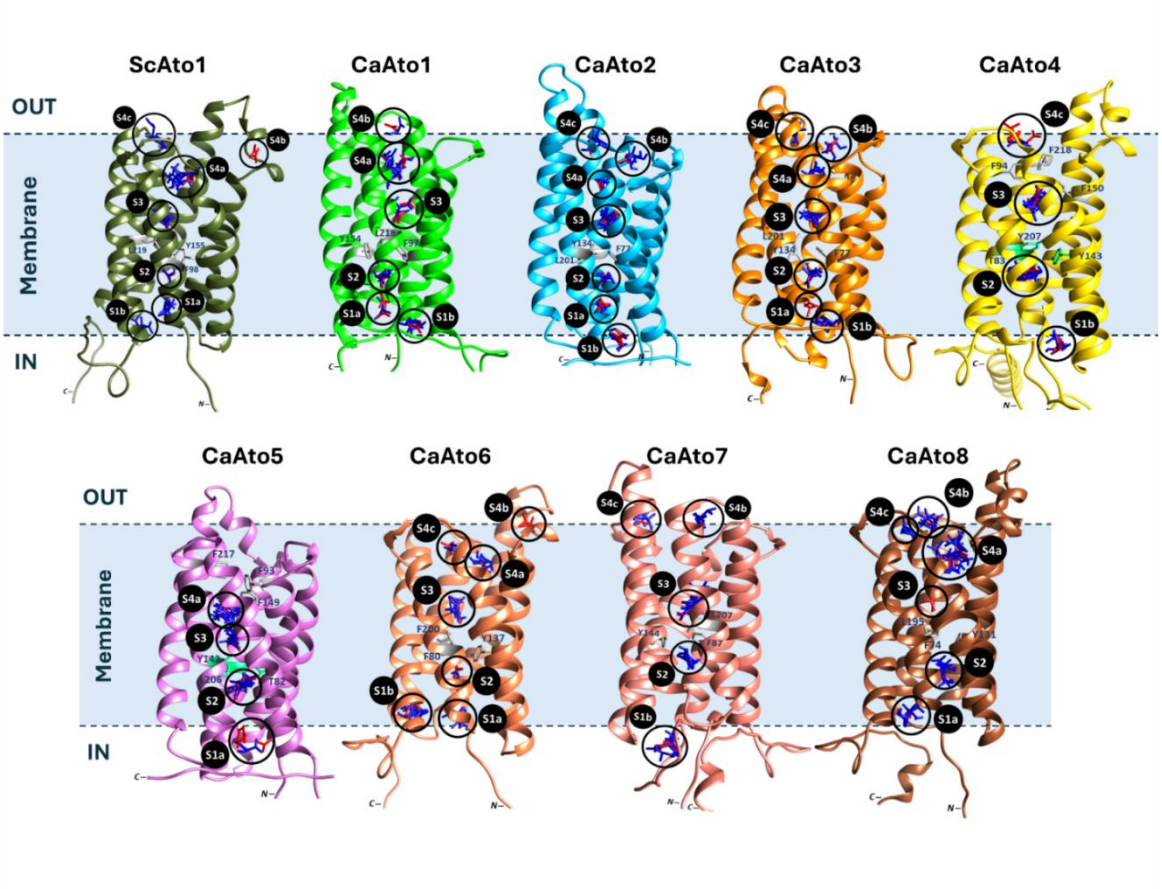

Figure 3. 3D structure and molecular docking of ScAto1 and CaAto1-8 with acetate and lactate as substrates. Predicted binding sites for acetate and lactate were shown with S1 to S4. Site S1 is located at the cytoplasmic vestibule, Sites S2 and S3 are located inside the main pore, and Site S4 is located at the periplasmic vestibule. Localization of the N- and C-terminal of the proteins is shown. Acetate and lactate ligands are presented in red and blue respectively.

3.4 Specific *C. albicans* Atos are localized to the plasma membrane in the presence of acetate and lactate

To study their expression and sub-cellular localization, we generated C-terminal GFP fusions for all ten Ato proteins in *C. albicans* (Table 2). The expression of these Ato-GFP fusions was examined during growth in the absence (YNB) or presence of lactic or acetic acid. Only Ato1-GFP, Ato2-GFP, Ato3-GFP and Ato6-GFP were expressed at detectable levels (Figure 4A, B and C). Ato6-GFP was detectable in the plasma membrane (PM) after prolonged growth on lactate (24 h). Ato1-GFP, Ato2-GFP and Ato3-GFP were detected in PM after 5hof derepression in acetic or lactic acid as well as in the YNB control (Figure 4A, B and C). After 5h, Ato1-GFP and Ato2-GFP signals in PM were similar, while Ato3-GFP was expressed at lower levels under all of the conditions tested. After 24 h, Ato1-GFP and Ato2-GFP increased in the PM, as did the amount of fluorescence associated with the vacuolar lumen, suggesting a rise in the turnover of these proteins. At 24 h, Ato3-GFP was localized mainly in the vacuole.

368 To clarify the roles of the lactate and acetate in the expression levels of Ato1, Ato2, Ato3 and Ato6,
369 Western-blot analyses using total protein extracts were performed (Figure 4D). Quantification of the
370 protein levels revealed that neither acetate nor lactate significantly changed the amount of Ato1. This was
371 rather surprising given that we have directly demonstrated that Ato1 is the main transporter responsible
372 for radiolabeled acetate uptake (Alves et al., 2025, unpublished data, manuscript under review). On the
373 other hand, carboxylic acids induced a significant increase in the expression of Ato2 (Figure 4D), suggesting
374 that besides Ato1, Ato2 might play a critical role in the uptake or utilization of weak organic acids. Acetate
375 also led to a decrease in Ato3 levels, but lactate did not change the Ato3 expression compared to the YNB
376 control condition (Figure 4D). Ato6, showed low levels of expression at 5h with no considerable
377 differences between the tested conditions. No signals were observed for Ato4-GFP, Ato5-GFP, Ato7-GFP,
378 Ato8-GFP, Ato9-GFP and Ato10-GFP in response to acetate or lactate (Figure 4). This suggests that these
379 transporters might be involved in the uptake of different substrates or be expressed in response to other
380 stimuli. Noticeably, our *in-silico* analysis revealed no appropriate lactate or acetate binding sites in these
381 proteins (Figure 3).

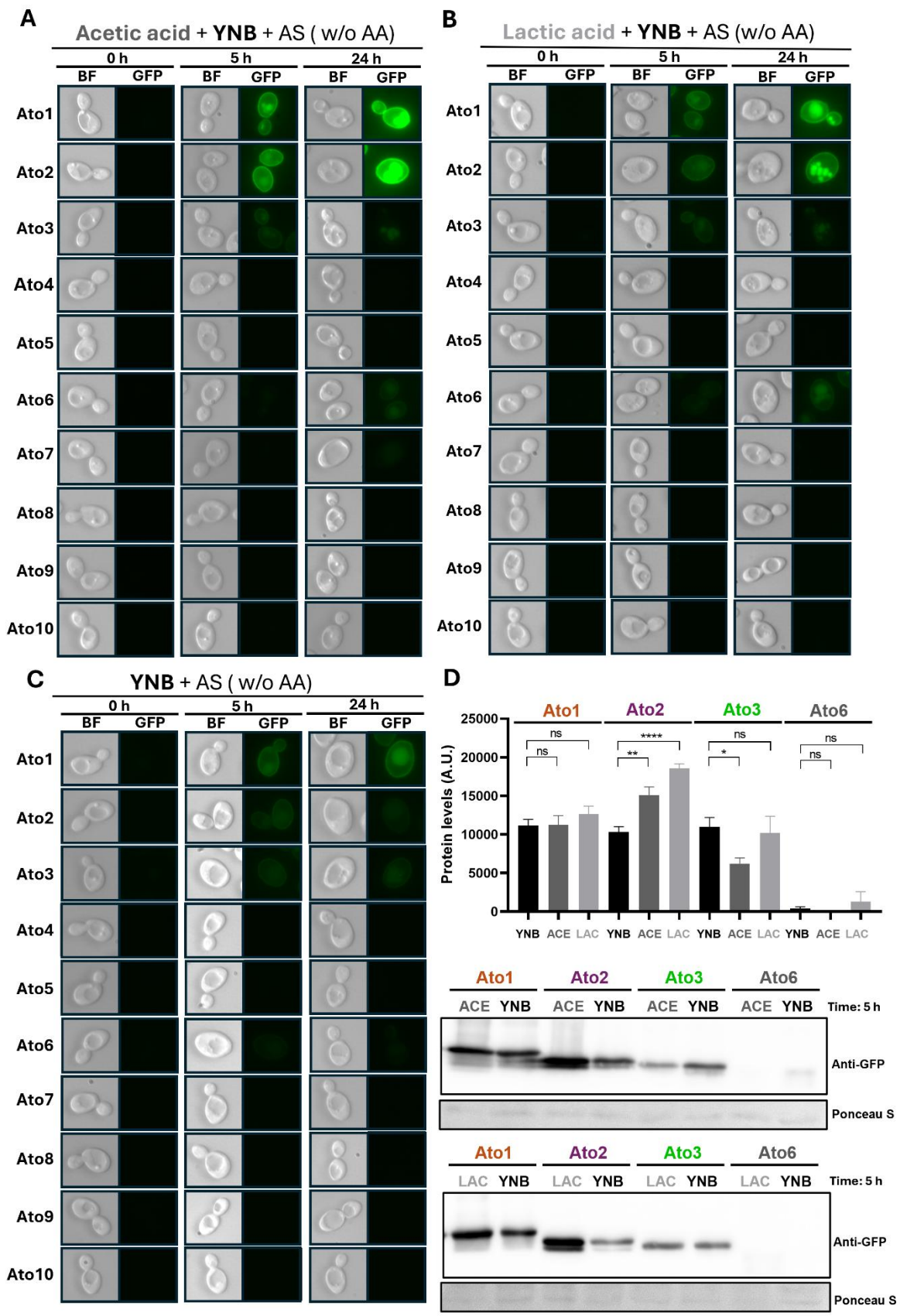
A
Acetic acid + YNB + AS (w/o AA)
0 h
5 h
24 h
BF
GFP
Ato1
Ato2
Ato3
Ato4
Ato5
Ato6
Ato7
Ato8
Ato9
Ato10
B
Lactic acid + YNB + AS (w/o AA)
C
YNB + AS (w/o AA)
D
Protein levels (A.U.)
25000
20000
15000
10000
5000
0
ns
****
**
*
YNB
ACE
LAC
Time: 5 h
Anti-GFP
Ponceau S

382

383 **Figure 4. Subcellular localization of Atos-GFP proteins in live *C. albicans* cells grown on different carbon sources.** *C. albicans*
384 cells grown in 50 mL SM medium supplemented with 0.2 % (w/v) glucose to exponential phase. They were washed then with
385 deionized water and then transferred, to fresh minimal media containing different carbon sources: (**A**) 0.1 % (v/v) acetic acid pH
386 6.0, (**B**) 0.1 % (v/v) lactic acid pH 5.0 and (**C**) without any carbon source (SM: 0.67% w/v YNB with ammonium sulphate). Samples
387 were collected after 0-, 5- and 24-hours induction, to examine cells by epifluorescence microscopy. Cell cultures were grown with
388 aeration 200 rpm, at 30 °C (**D**) At the time-point 5h, protein extracts were prepared for western immunoblotting with an anti-
389 GFP antibody. Quantification of the protein levels in arbitrary units (A.U.) were done using ImageJ software (version 1.53k). Error
390 bars correspond to standard error of the mean (SEM) of at least three independent experiments. ns, not significant; *P=0.0255;
391 **P=0.0014; ****P<0.0001 (unpaired t-test (two-tailed) using Prism 8). Ponceau S staining was used as a transference and loading
392 control. The abbreviations BF and GFP refer to "Bright-Field" and "Green Fluorescent Protein," respectively

393 **3.5 Deletion of *ATO1* affects the localization and expression of Ato2 and Ato3**

394 To explore potential functional cooperative interactions between Ato proteins, we constructed *ato1, ato2*
395 or *ato3* deletions in the Ato1- Ato2- or Ato3-GFP backgrounds in *C. albicans* (Table 2). The expression and
396 subcellar localization of Ato-GFP proteins in these strains were examined in response to acetate or lactate
397 (Figure 5).
398 The deletion of *ATO2* did not interfere with Ato1-GFP or Ato3-GFP expression under any of the conditions
399 tested as demonstrated by GFP fluorescence (Figure 5A, B and C) and Western blotting (Figure 5D).
400 However, deleting *ATO3* had a slight impact in expression of Ato1 only in YNB condition (Figure 5D), but
401 did not show any influence in Ato2 protein levels in all the conditions tested (Figure 5F). Most
402 interestingly, under all of the conditions tested, the deletion of *ATO1* had a pronounced impact on the
403 expression and PM localization of Ato2-GFP and Ato3-GFP (Figure 5A, B and C, rows 5 and 8). The *ato1Δ*
404 mutant exhibited Ato2-GFP localization at the cortical and nuclear endoplasmic reticulum (ER) after 5-h,
405 followed by complete abolishment of Ato2 expression after 24 hours in the presence of acetic acid.
406 Moreover, the deletion of *ATO1* resulted in a complete loss of Ato2-GFP and Ato3-GFP expression in YNB
407 and in response to lactate (Figure 5, B and C**,** lines 5 and 8). These results were consistent with the
408 Western blot analysis, which showed either no detectable bands or only faint bands for both Ato2 and
409 Ato3 under these conditions. Also, acetate led to a decrease in Ato3 levels, and lactate led to a slight
410 increase in Ato6 levels, but these changes were not statistically significant. In addition, Western blotting
411 revealed interesting effects upon Ato2-GFP expression in the presence of acetate and lactate (Figure 5E).
412 In the wild-type background, Ato2-GFP appeared as two bands, possibly representing non-phosphorylated
413 and phosphorylated versions of Ato2. However, in the *ato1* mutant, only the lower band was observed in
414 response to acetate or lactate (Figure 5E). This suggests that Ato1 might regulate Ato2 by controlling
415 (directly or indirectly) its post-translation modification. Indeed, Ato2 contains 20 potential
416 phosphorylation sites including 12 serine and 8 threonine residues (Figure S9). Four serine residues at
417 positions 6, 9, 13, and 28 showed approximately maximum scores (1.000), suggesting a very high
418 probability of phosphorylation. Importantly, these residues are localized within the N-terminal region of

419 the protein. Several phosphorylation sites have been reported in the N-terminal region of Ato proteins in
420 *S. cerevisiae* (60). These findings reinforce that CaAto2 potentially undergoes phosphorylation. Noticeably
421 also, after 5h in acetate, the presence of the lower Ato2-GFP band correlated with fluorescence in the
422 endoplasmic reticulum (Figure 5A, line 5), suggesting that unmodified Ato2-GFP fails to be targeted to the
423 PM and that this modification probably occurs at ER. In the absence of Ato1, neither form of Ato2-GFP
424 was observed without acetate or lactate (Figure 5E, YNB control), reflecting the lack of fluorescence under
425 these conditions at 24 h (Figure 5, B and C**,** line 5). The same was true for Ato3-GFP in *ato1* cells (Figure 5,
426 B and C**,** line 8; Figure 5F). Overall, Ato1 appears to be required for stable expression and proper
427 localization of Ato2 and Ato3 in *C. albicans*. This would be compatible with physical interactions between
428 Ato1, Ato2 and Ato3 and possibly their formation of heterohexameric complexes in *C. albicans.* Some
429 AceTr family members are thought to form homohexamers: ecSatP and ckSatP (33,34) and possibly
430 ScAto1, ScAto2 and ScAto3 (61,62). However, there is evidence suggesting that ScAto1 and ScAto2 interact
431 physically at the plasma membrane (57).
432

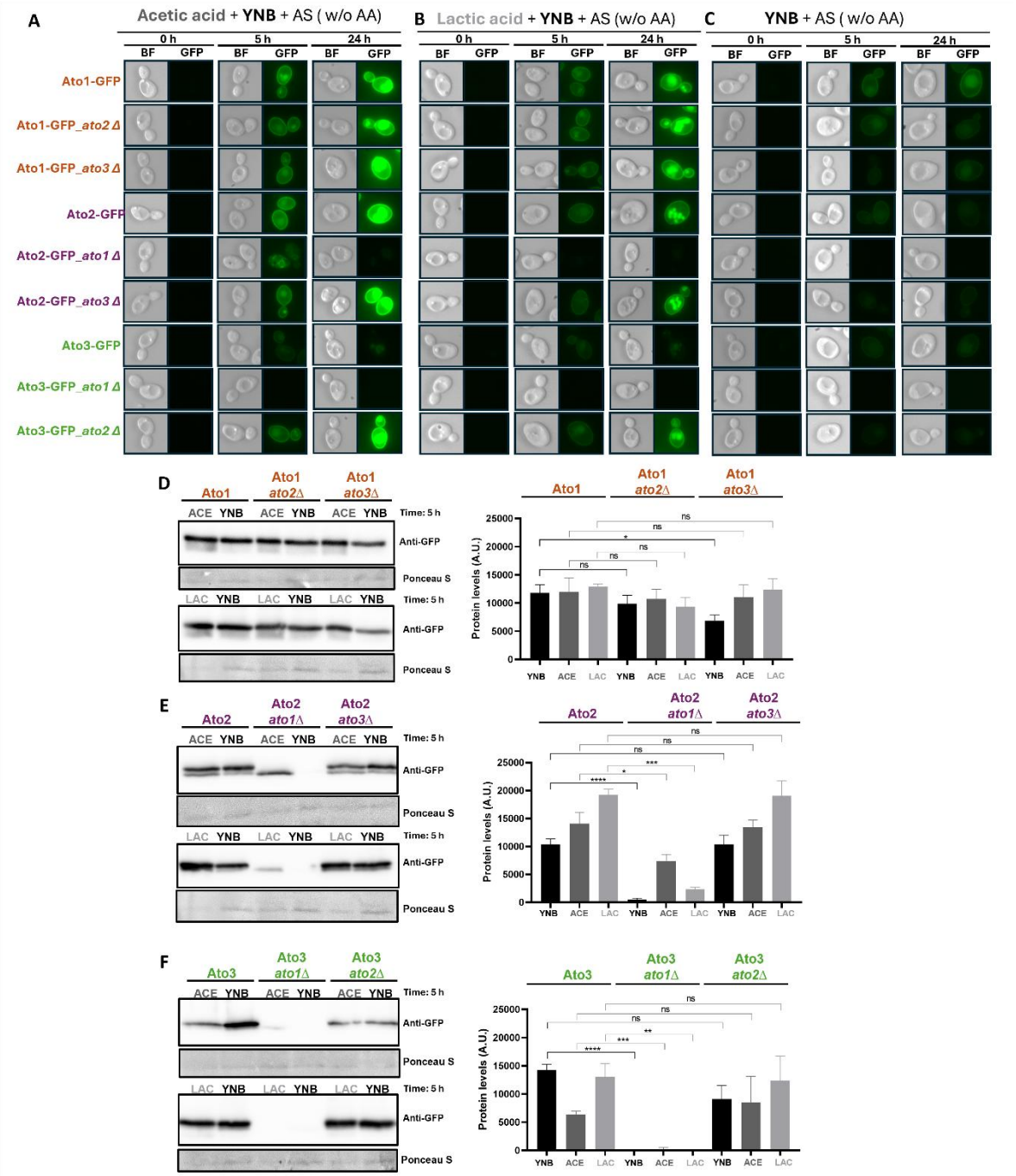

Figure 5. Subcellular localization of the indicted Atos-GFP in *C. albicans*. WT and *ato*-mutant cells. *C. albicans* cells grown in 50 mL SM medium supplemented with 0.2 % (w/v) glucose to exponential phase. They were washed then with deionized water and then transferred, to fresh minimal media containing different carbon sources: **(A)** 0.1 % (v/v) acetic acid pH 6.0, **(B)** 0.1 % (v/v) lactic acid pH 5.0 and **(C)** without any carbon source (SM: 0.67% w/v YNB with ammonium sulphate). Samples were collected after 0-, 5- and 24-hours induction, to examine cells by epifluorescence microscopy. Cell cultures were grown with aeration 200 rpm, at 30 °C (**D-F**) At the time-point 5h, protein extracts were prepared for western immunoblotting with an anti-GFP antibody. Quantification of the protein levels in arbitrary units (A.U.) were done using ImageJ software (version 1.53k). Error bars

correspond to standard error of the mean (SEM) of at least three independent experiments. ns, not significant; *P=0.0183-0.0455; **P=0.0014-0.0054; ***P=0.0001-0.0008; ****P<0.0001 (unpaired t-test (two-tailed) using Prism 8). Ponceau S staining was used as a transference and loading control. The abbreviations BF and GFP refer to "Bright-Field" and "Green Fluorescent Protein," respectively.

3.6 Vertebrate ATOs are characterized by transport domain duplications and a gene fusion event

Taxonomic distribution studies showed that AceTr/Ato proteins are present in both prokaryotic and eukaryotic members (26,58), but not in metazoan. These studies employed BLASTp searches, using known Ato proteins as baits (EcSatP from *E. coli,* AceP from *M. acetivorans,* Ady2 from *S. cerevisiae,* or Atos from *Cyberlindnera jadinii*). To further investigate, we used a sensitive hmmsearch and the PFAM HMM-profile (PF01184) of the AceTr transporter family to collect fungal and metazoan sequences. This revealed that AceTr/Ato family members are widespread within *Bilateria* and particularly vertebrates (Figure 6 and Figure S7). Vertebrate ATOs form two clades with representatives from every major lineage, except mammals (Figure 6). A small number of protostome sequences can be identified within the vertebrate clade, suggesting possible horizontal gene transfer. Notably, vertebrate ATOs and their close invertebrate homologs are *circa* 900 amino acids in length, contrasting with the 200-300 amino acid length of their fungal and prokaryotic counterparts (Figure 1) (33,34). Surprisingly, almost all of the vertebrate sequences that we identified have a C-terminal fusion to a Sua5/YciO/YrdC domain in addition to the Gpr1/Fun34/YaaH domains that characterize the AceTr/Ato transporter family (Figure 6 and Figure S6). This domain is not present in the bacterial SatP (Figure 6) or in the protostome and fungal clades (Figure S7). Sua5/YciO/YrdC proteins are annotated as threonyl-carbamoyl-AMP synthetases, which attach a threonyl-carbamoyl group to A37 (t6A37) of a tRNA (63). This tRNA modification is common for tRNAs that have A/U-rich anticodons, helping to stabilize their codon-anticodon interactions (64). Loss of threonyl-carbamoyl-AMP synthetase (Sua5) leads to increased rates of translational frameshifting and stop codon read-through in yeast, underlining the importance of the t6A37 modification for translational fidelity (65).

Comparing the experimentally resolved EcSatP structure from *E. coli* (33) with the AlphaFold 2.0 (44) predictions of some vertebrate ATO proteins revealed that they consist of three Gpr1/Fun34/YaaH domains (six helices each) fused in tandem (Figure 6B). HMM-scan for the Gpr1/Fun34/YaaH HMM-profile in vertebrate sequences returns three domain hits for some of them (Figure S6). Structural investigation of proteins that produce less than three hits revealed that they possess three copies of the six-helix Gpr1/Fun34/YaaH fold (Figure S6).

TM-align superposition of the vertebrate A0A3B3D9A3 from *Oryzias melastigma* (chordate fish) with SatP revealed strong structural similarity with an RMSD of 2.53 Å and a TM-score of 0.82. Superimposed structures of the two proteins are presented in Figure 6. Interestingly, SatP crystals have revealed a homohexameric structure (33) (Figure 6C). Observing the duplicated Gpr1/Fun34/YaaH domains of vertebrate Atos, we hypothesized that two interacting protomers could be arranged in a six-domain ring similar to the one formed by SatP. Hence, cross-kingdom conservation of the six-domain ring structure of Ato proteins suggests that its functional relevance persists in vertebrate homologs.

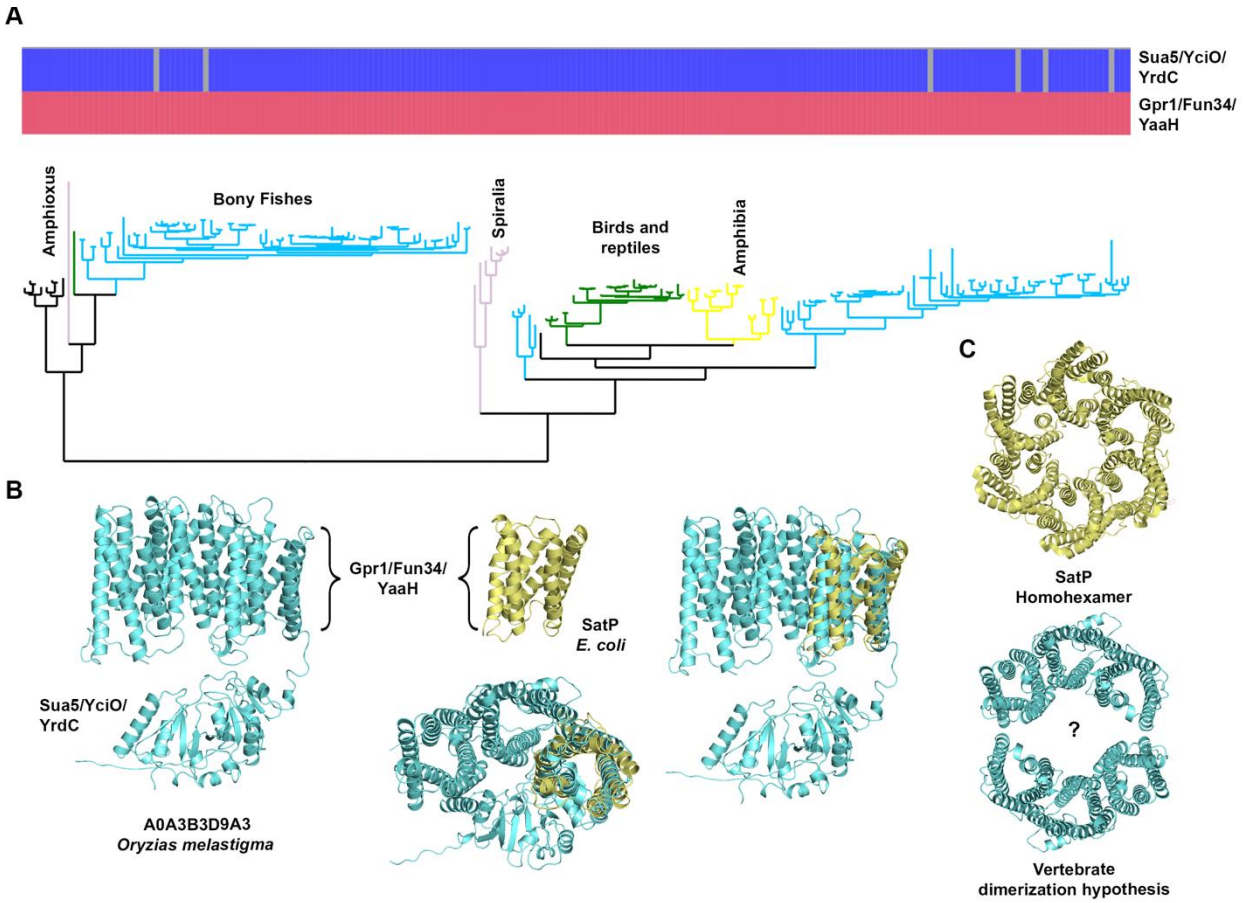

Figure 6. Vertebrate ATO phylogeny and structure. A. Phylogeny and domain composition of vertebrate ATO proteins. Domain presence is denoted as blue or red and domain absence with grey. Tree branches are colored based on taxonomy. Full metazoan phylogeny can be seen in figure S6. **B.** Alphafold 2.0 structure prediction of a vertebrate ATO protein (cyan) and crystal structure of SatP (yellow). The triplication of the Gpr1/Fun34/YaaH domain is apparent when structures are superimposed. **C.** Dimerization hypothesis of the vertebrate ATO homologs based on the experimentally determined SatP hexamer.

4. Conclusion

Our study investigated the expansion, structural divergence, and functional specialization of the ATO protein family in *Candida species*, with a focus on *C. albicans*. We found that key motifs such as NPAPLGL

489 and FLY are conserved among Ato homologs. However, significant variations exist in the pore
490 constrictions, which are potentially responsible for their substrate specificity. Our findings revealed that
491 Ato2 expression is markedly induced under acetate and lactate growth conditions, with prominent
492 localization at the plasma membrane. Additionally, the expression of Ato2 and Ato3 at the plasma
493 membrane was dependent upon Ato1, which is consistent with the idea that functional Ato proteins
494 assemble as heterooligomeric complexes in *C. albicans*. This is further supported by the observation that
495 Ato1 and Ato2 interact physically in *S. cerevisiae* (61,62). In addition, the bacterial homolog SatP has been
496 reported to function as a homohexamer (33). This suggests that oligomerization may be a conserved
497 feature required for the proper activity of these transporter proteins, whether through homomeric or
498 heteromeric assembly. Our *in-silico* and expression analysis suggested that Ato4, Ato5, Ato7 and Ato8 are
499 not involved in the utilization of lactate or acetate and therefore may have different substrate specificities.
500 Our findings regarding the fusion of Ato members with Sua5 enzyme in vertebrates remain elusive. We
501 hypothesize that the cytoplasmic region of vertebrate Ato members could catalyze a reaction similar to
502 carbamoyl-AMP synthesis. However, its exact biochemical function in vertebrates needs further
503 investigation. Another hypothesis is that a fusion of an enzyme with a functionally related transporter
504 may directly link substrate import to its metabolic assimilation, enhancing the rate and/or efficiency of
505 downstream enzymatic reactions.
506 In summary, this work provides new insights into the structure and potential function of Ato members in
507 *C. albicans* but also serves as a basis for further studies in higher eukaryotes.

508 **References:**

509 1. Parambath S, Dao A, Kim HY, Zawahir S, Alastruey Izquierdo A, Tacconelli E, et al. *Candida albicans*—
510 A systematic review to inform the World Health Organization Fungal Priority Pathogens List. Medical
511 Mycology. 2024 Jun 1;62(6):myae045.

512 2. Katsipoulaki M, Stappers MHT, Malavia-Jones D, Brunke S, Hube B, Gow NAR. *Candida albicans* and
513 *Candida glabrata*: global priority pathogens. Microbiology and Molecular Biology Reviews [Internet].
514 2024 Jun 27 [cited 2025 Apr 15]; Available from: https://journals.asm.org/doi/10.1128/mmbr.00021-
515 23

516 3. Lass-Flörl C, Steixner S. The changing epidemiology of fungal infections. Molecular Aspects of
517 Medicine. 2023 Dec 1;94:101215.

518 4. Osei Sekyere J. *Candida auris*: A systematic review and meta-analysis of current updates on an
519 emerging multidrug-resistant pathogen. MicrobiologyOpen. 2018;7(4):e00578.

520 5. Diekema D, Arbefeville S, Boyken L, Kroeger J, Pfaller M. The changing epidemiology of healthcare-
521 associated candidemia over three decades. Diagnostic Microbiology and Infectious Disease. 2012 May
522 1;73(1):45–8.

523 6. Pfaller MA, Diekema DJ. Epidemiology of Invasive Candidiasis: a Persistent Public Health Problem.
524 Clinical Microbiology Reviews. 2007 Jan;20(1):133–63.

525 7. Singh S, Sobel JD, Bhargava P, Boikov D, Vazquez JA. Vaginitis Due to *Candida krusei:* Epidemiology,
526 Clinical Aspects, and Therapy. Clinical Infectious Diseases. 2002 Nov 1;35(9):1066–70.

527 8. Alves R, Sousa-Silva M, Vieira D, Soares P, Chebaro Y, Lorenz MC, et al. Carboxylic acid transporters in
528 *candida* pathogenesis. mBio. 2020;11(3):1–11.

529 9. Pappas PG, Lionakis MS, Arendrup MC, Ostrosky-Zeichner L, Kullberg BJ. Invasive candidiasis. Nat Rev
530 Dis Primers. 2018 May 11;4(1):1–20.

531 10. Tsai MH, Hsu JF, Yang LY, Pan YB, Lai MY, Chu SM, et al. Candidemia due to uncommon *Candida*
532 species in children: new threat and impacts on outcomes. Sci Rep. 2018 Oct 15;8(1):15239.

533 11. Bougnoux ME, Brun S, Zahar JR. Healthcare-associated fungal outbreaks: New and uncommon
534 species, New molecular tools for investigation and prevention. Antimicrob Resist Infect Control. 2018
535 Mar 27;7(1):45.

536 12. Kohlenberg A, Struelens MJ, Monnet DL, Plachouras D. *Candida auris:* epidemiological situation,
537 laboratory capacity and preparedness in European Union and European Economic Area countries,
538 2013 to 2017. Euro Surveill. 2018 Mar 29;23(13):18–00136.

539 13. Alves R, Barata-Antunes C, Casal M, Brown AJP, Dijck PV, Paiva S. Adapting to survive: How *Candida*
540 overcomes host-imposed constraints during human colonization. PLOS Pathogens. 2020 May
541 21;16(5):e1008478.

14. Cauchie M, Desmet S, Lagrou K. *Candida* and its dual lifestyle as a commensal and a pathogen. Research in Microbiology. 2017 Nov 1;168(9):802–10.

15. Mayer FL, Wilson ,Duncan, and Hube B. *Candida albicans* pathogenicity mechanisms. Virulence. 2013 Feb 15;4(2):119–28.

16. Ene IV, Brunke S, Brown AJP, Hube B. Metabolism in Fungal Pathogenesis. Cold Spring Harb Perspect Med. 2014 Dec 1;4(12):a019695.

17. Childers DS, Raziunaite I, Avelar GM, Mackie J, Budge S, Stead D, et al. The Rewiring of Ubiquitination Targets in a Pathogenic Yeast Promotes Metabolic Flexibility, Host Colonization and Virulence. PLOS Pathogens. 2016 Apr 13;12(4):e1005566.

18. Johnston M. Feasting, fasting and fermenting: glucose sensing in yeast and other cells. Trends in Genetics. 1999 Jan 1;15(1):29–33.

19. impact of the Fungus-Host-Microbiota interplay upon *Candida albicans* infections: current knowledge and new perspectives | FEMS Microbiology Reviews | Oxford Academic [Internet]. [cited 2025 Apr 15]. Available from: https://academic.oup.com/femsre/article/45/3/fuaa060/6000215

20. Padder SA, Ramzan ,Asiya, Tahir ,Inayatullah, Rehman ,Reiaz ul, and Shah AH. Metabolic flexibility and extensive adaptability governing multiple drug resistance and enhanced virulence in *Candida albicans*. Critical Reviews in Microbiology. 2022 Jan 2;48(1):1–20.

21. Morrison DJ, and Preston T. Formation of short chain fatty acids by the gut microbiota and their impact on human metabolism. Gut Microbes. 2016 May 3;7(3):189–200.

22. The *Candida albicans* ATO Gene Family Promotes Neutralization of the Macrophage Phagolysosome | Infection and Immunity [Internet]. [cited 2025 Apr 15]. Available from: https://journals.asm.org/doi/full/10.1128/iai.00984-15

23. The carboxylic acid transporters Jen1 and Jen2 affect the architecture and fluconazole susceptibility of *Candida albicans* biofilm in the presence of lactate: Biofouling: Vol 33, No 10 [Internet]. [cited 2025 Apr 15]. Available from: https://www.tandfonline.com/doi/abs/10.1080/08927014.2017.1392514?casa_token=H3PeX9KfO5QAAAAA:HjLWFZk1zvSSt_a0NSv5VrLGZj4d0bgz_ft7SEGjexDDG68Y96ZpWZgmOrZGRDhLqFJBV4Nnt4IZ

24. Transport of carboxylic acids in yeasts | FEMS Microbiology Reviews | Oxford Academic [Internet]. [cited 2025 Apr 15]. Available from: https://academic.oup.com/femsre/article/32/6/974/2683394

25. Casal M, Queirós O, Talaia G, Ribas D, Paiva S. Carboxylic Acids Plasma Membrane Transporters in *Saccharomyces cerevisiae*. In: Ramos J, Sychrová H, Kschischo M, editors. Yeast Membrane Transport [Internet]. Cham: Springer International Publishing; 2016 [cited 2025 Apr 15]. p. 229–51. Available from: https://doi.org/10.1007/978-3-319-25304-6_9

26. Ribas D, Soares-Silva I, Vieira D, Sousa-Silva M, Sá-Pessoa J, Azevedo-Silva J, et al. The acetate uptake transporter family motif “NPAPLGL(M/S)” is essential for substrate uptake. Fungal Genetics and Biology. 2019 Jan 1;122:1–10.

27. Rabitsch KP, Tóth A, Gálová M, Schleiffer A, Schaffner G, Aigner E, et al. A screen for genes required for meiosis and spore formation based on whole-genome expression. Current Biology. 2001 Jul 10;11(13):1001–9.

28. Sá-Pessoa J, Amillis S, Casal M, Diallinas G. Expression and specificity profile of the major acetate transporter AcpA in *Aspergillus nidulans*. Fungal Genetics and Biology. 2015 Mar 1;76:93–103.

29. Tzschoppe K, Augstein A, Bauer R, Kohlwein SD, Barth G. trans-dominant mutations in the GPR1 gene cause high sensitivity to acetic acid and ethanol in the yeast *Yarrowia lipolytica*. Yeast. 1999 Nov 1;15(15):1645–56.

30. Paiva S, Devaux F, Barbosa S, Jacq C, Casal M. Ady2p is essential for the acetate permease activity in the yeast *Saccharomyces cerevisiae*. Yeast. 2004 Feb 1;21(3):201–10.

31. Sá-Pessoa J, Paiva S, Ribas D, Silva IJ, Viegas SC, Arraiano CM, et al. SATP (YaaH), a succinate–acetate transporter protein in *Escherichia coli*. Biochemical Journal. 2013 Aug 29;454(3):585–95.

32. Rendulić T, Alves J, Azevedo-Silva J, Soares-Silva I, Casal M. New insights into the acetate uptake transporter (AceTr) family: Unveiling amino acid residues critical for specificity and activity. Computational and Structural Biotechnology Journal. 2021;19:4412–25.

33. Sun P, Li J, Zhang X, Guan Z, Xiao Q, Zhao C, et al. Crystal structure of the bacterial acetate transporter SatP reveals that it forms a hexameric channel. Journal of Biological Chemistry. 2018;293(50):19492–500.

34. Qiu B, Xia B, Zhou Q, Lu Y, He M, Hasegawa K, et al. Succinate-acetate permease from *Citrobacter koseri* is an anion channel that unidirectionally translocates acetate. Cell Research. 2018;28(6):644–54.

35. Genomic Expression Programs in the Response of Yeast Cells to Environmental Changes | Molecular Biology of the Cell [Internet]. [cited 2025 Apr 15]. Available from: https://www.molbiolcell.org/doi/full/10.1091/mbc.11.12.4241

36. Boer VM, Winde JH de, Pronk JT, Piper MDW. The Genome-wide Transcriptional Responses of *Saccharomyces cerevisiae* Grown on Glucose in Aerobic Chemostat Cultures Limited for Carbon, Nitrogen, Phosphorus, or Sulfur *. Journal of Biological Chemistry. 2003 Jan 31;278(5):3265–74.

37. Danhof HA LM. The *Candida albicans* ATO Gene Family Promotes Neutralization of the Macrophage Phagolysosome. Infect Immun. 2015;83:4416–26.

38. Slavena V, J. CA, A. DH, R. CJ, Huaijin Z, C. LM. The Fungal Pathogen *Candida albicans* Autoinduces Hyphal Morphogenesis by Raising Extracellular pH. mBio. 2011 May 17;2(3):e00055-11.

39. MAFFT: a novel method for rapid multiple sequence alignment based on fast Fourier transform | Nucleic Acids Research | Oxford Academic [Internet]. [cited 2025 Apr 22]. Available from: https://academic.oup.com/nar/article/30/14/3059/2904316

40. Capella-Gutiérrez S, Silla-Martínez JM, Gabaldón T. trimAl: a tool for automated alignment trimming in large-scale phylogenetic analyses. Bioinformatics. 2009 Aug 1;25(15):1972–3.

41. IQ-TREE 2: New Models and Efficient Methods for Phylogenetic Inference in the Genomic Era | Molecular Biology and Evolution | Oxford Academic [Internet]. [cited 2025 Apr 22]. Available from: https://academic.oup.com/mbe/article/37/5/1530/5721363

42. Huerta-Cepas J, Serra F, Bork P. ETE 3: Reconstruction, Analysis, and Visualization of Phylogenomic Data. Molecular Biology and Evolution. 2016 Jun 1;33(6):1635–8.

43. Sievers F, Wilm A, Dineen D, Gibson TJ, Karplus K, Li W, et al. Fast, scalable generation of high-quality protein multiple sequence alignments using Clustal Omega. Mol Syst Biol. 2011 Oct 11;7:539.

44. Jumper J, Evans R, Pritzel A, Green T, Figurnov M, Ronneberger O, et al. Highly accurate protein structure prediction with AlphaFold. Nature. 2021;596(7873):583–9.

45. Varadi M, Anyango S, Deshpande M, Nair S, Natassia C, Yordanova G, et al. AlphaFold Protein Structure Database: Massively expanding the structural coverage of protein-sequence space with high-accuracy models. Nucleic Acids Research. 2022;50(D1):D439–44.

46. Smart OS, Neduvelil JG, Wang X, Wallace BA, Sansom MS. HOLE: a program for the analysis of the pore dimensions of ion channel structural models. J Mol Graph. 1996 Dec;14(6):354–60, 376.

47. Humphrey W, Dalke A, Schulten K. VMD: visual molecular dynamics. J Mol Graph. 1996 Feb;14(1):33–8, 27–8.

48. Wu M, Sun L, Zhou Q, Peng Y, Liu Z, Zhao S. Molecular Mechanism of Acetate Transport through the Acetate Channel SatP. Journal of Chemical Information and Modeling. 2019;59(5):2374–82.

49. Trott O, Olson AJ. AutoDock Vina: Improving the speed and accuracy of docking with a new scoring function, efficient optimization, and multithreading. Journal of Computational Chemistry. 2010 Jan 30;31(2):455–61.

50. Ribas D, ´ A-Pessoa JS, Soares-Silva I, Paiva S, Nygård Y, Nygård N, et al. Yeast as a tool to express sugar acid transporters with biotechnological interest. FEMS Yeast Research. 2017;17:5.

51. Blom N, Gammeltoft S, Brunak S. Sequence and structure-based prediction of eukaryotic protein phosphorylation sites1. Journal of Molecular Biology. 1999 Dec 17;294(5):1351–62.

52. Prediction of post-translational glycosylation and phosphorylation of proteins from the amino acid sequence - Blom - 2004 - PROTEOMICS - Wiley Online Library [Internet]. [cited 2025 May 24]. Available from: https://analyticalsciencejournals.onlinelibrary.wiley.com/doi/abs/10.1002/pmic.200300771

53. Nguyen N, Quail MMF, Hernday AD. An Efficient, Rapid, and Recyclable System for CRISPR-Mediated Genome Editing in *Candida albicans*. mSphere. 2017;2(2).

54. Van Genechten W, Demuyser L, Dedecker P, Van Dijck P. Presenting a codon-optimized palette of fluorescent proteins for use in *Candida albicans*. Scientific Reports. 2020;10(1):1–9.

55. Min K, Ichikawa Y, Woolford CA, Mitchell AP. *Candida albicans* Gene Deletion with a Transient CRISPR-Cas9 System. mSphere. 2016;1(3):e00130-16.

649 56. Walther A, Wendland J. An improved transformation protocol for the human fungal pathogen
650 *Candida albicans*. Curr Genet. 2003 Mar;42(6):339–43.

651 57. Volland C, Urban-Grimal D, Géraud G, Haguenauer-Tsapis R. Endocytosis and degradation of the yeast
652 uracil permease under adverse conditions. Journal of Biological Chemistry. 1994 Apr 1;269(13):9833–
653 41.

654 58. Sousa-Silva M, Soares P, Alves J, Vieira D, Casal M, Soares-Silva I. Uncovering Novel Plasma Membrane
655 Carboxylate Transporters in the Yeast *Cyberlindnera jadinii*. Journal of Fungi. 2022;8(1).

656 59. Baldi N, De Valk SC, Sousa-Silva M, Casal M, Soares-Silva I, Mans R. Evolutionary engineering reveals
657 amino acid substitutions in Ato2 and Ato3 that allow improved growth of *Saccharomyces cerevisiae*
658 on lactic acid. FEMS Yeast Research. 2021;21(4):1–12.

659 60. Reinders J, Wagner K, Zahedi RP, Stojanovski D, Eyrich B, Laan M van der, et al. Profiling
660 Phosphoproteins of Yeast Mitochondria Reveals a Role of Phosphorylation in Assembly of the ATP
661 Synthase *. Molecular & Cellular Proteomics. 2007 Nov 1;6(11):1896–906.

662 61. Řičicová M, Kučerová H, Váchová L, Palková Z. Association of putative ammonium exporters Ato with
663 detergent-resistant compartments of plasma membrane during yeast colony development: pH affects
664 Ato1p localisation in patches. Biochimica et Biophysica Acta (BBA) - Biomembranes. 2007 May
665 1;1768(5):1170–8.

666 62. Strachotová D, Holoubek A, Kučerová H, Benda A, Humpolíčková J, Váchová L, et al. Ato protein
667 interactions in yeast plasma membrane revealed by fluorescence lifetime imaging (FLIM). Biochimica
668 et Biophysica Acta (BBA) - Biomembranes. 2012 Sep 1;1818(9):2126–34.

669 63. Thiaville PC, El Yacoubi B, Köhrer C, Thiaville JJ, Deutsch C, Iwata-Reuyl D, et al. Essentiality of
670 threonylcarbamoyladenosine (t6A), a universal tRNA modification, in bacteria. Molecular
671 Microbiology. 2015;98(6):1199–221.

672 64. Murphy FV, Ramakrishnan V, Malkiewicz A, Agris PF. The role of modifications in codon discrimination
673 by tRNALysUUU. Nat Struct Mol Biol. 2004 Dec;11(12):1186–91.

674 65. Lin CA, Ellis ,Steven R., and True HL. The Sua5 Protein Is Essential for Normal Translational Regulation
675 in Yeast. Molecular and Cellular Biology. 2010 Jan;30(1):354–63.

676